Investigation of an Alternative APFC Control with no Sensing of Line Voltage Based on a Triangular Modulation Carrier

Alexander Abramovitz
Sami Shamoon College of Engineering
71 Bazel st.
Beer-Sheva, 84100 Israel,
alexabr@sce.ac.il

Michael Evzelman and Sam Ben-Yaakov
Ben-Gurion Univ. of the Negev
Beer-Sheva, 84105 Israel
sby@ee.bgu.ac.il; evzelman@ee.bgu.ac.il
Website: www.ee.bgu.ac.il\~pel\

***Abstract*-An alternative control method for a Boost Active Power Factor Corrector (APFC) operating in Continuous Conduction Mode is presented, analyzed and verified by simulation and experiments. The proposed APFC scheme employs average current control to shape the input current. The power level is adjusted by modulating the amplitude of a triangular carrier as a function of the outer loop error signal. The proposed APFC does not require neither line voltage sensing nor an input voltage reference circuitry. The theoretical predictions are well supported by simulation and experimental results. The experimental results demonstrate some improved performance at low power levels as compared to other methods of APFC without sensing of input voltage.**

***Index Terms*— AC-DC power conversion, power factor, PFC.**

I. INTRODUCTION

Over the past few years, a variety of input current shaping methodologies were developed for single phase APFC to meet the line harmonics norms [1] - [7]. In particularly, APFC without line voltage sensing, [8-13], stands out as a robust, technologically simple and cost-effective solution. A simple and clear physical insight into the principle of operation of the current loop of this class of APFCs was suggested in [14].

The purpose of this paper is to present an alternative approach for the implementation of the APFC of this control class. The idea, presented here, describes an average current mode APFC regulated by an Amplitude Modulated Triangular Carrier which leads to different controller implementation. The Improved APFC potentially overcomes some of the deficiencies of previously reported systems based on a sawtooth ramp carrier counterpart. The paper presents theoretical concepts, simulation and experimental results.

II. REVIEW OF THE BOOST APFC PROGRAMMING LAW

The proposed APFC block diagram is shown at Fig. 1. The goal of APFC systems is to shape the averaged input current, $<i_{in}(t)>$ to be proportional to the line voltage, $v_{in}(t)$, while maintaining a constant output voltage, V_O, for a DC load . The

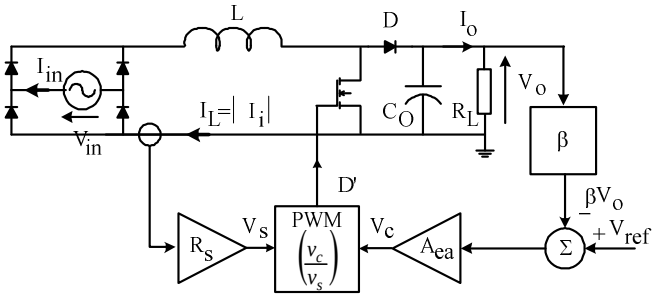

Figure 1. Single phase Boost based APFC with no sensing of input voltage.

first goal can be met by making the input of the APFC stage resistive:

$$R_e = \frac{v_{in}(t)}{\langle i_{in}(t)\rangle} = \frac{V_{rms}^2}{P_o} \tag{1}$$

Where V_{rms}, is the line RMS voltage, R_e, is the emulated resistance seen into the APFC line terminals and P_o is the average power drown from the AC line. Applying the definitions above yields the Off-Duty Cycle (D') Programming Law for the Boost based APFC operated in the CCM as:

$$D' \cong \frac{v_{in}(t)}{V_o} \cong \frac{R_e\langle i_{in}(t)\rangle}{V_o} \cong \frac{1}{V_o}\left(\frac{V_{rms}^2}{P_o}\right)\langle i_{in}(t)\rangle \tag{2}$$

This formulation is similar to that reported by [10-14].

III. IMPLEMENTATION OF THE PWM MODULATOR

The APFC system of Fig. 1 senses the Boost inductor current, i_L, by a current sensing network with R_S as the low frequency gain, including both the sense resistor and current amplifier – if used. Thus, the low frequency average component, $<v_s>$, at the output of the current sensing network, is proportional to the average input current i_L:

$$\langle v_s \rangle = R_S \langle i_L \rangle \tag{3}$$

978-1-4244-1874-9/08/$25.00 ©2008 IEEE

The Off-Duty cycle signal can be generated by comparing the <v_s> signal to a triangular modulating wave as shown in Fig. 2:

$$D' = \frac{\langle v_s \rangle}{V_{pk}} \tag{4}$$

By comparing (4) with (2), the required peak voltage, V_{pk}, for emulating a restive input is thus:

$$V_{pk} = \left(R_s \frac{V_o}{V_{rms}^2} \right) P_o = \left(R_s \frac{V_o^2}{V_{rms}^2} \right) I_o \tag{5}$$

The peak voltage, V_{pk}, can be automatically adjusted in closed loop by making it to follow the voltage error amplifier voltage, V_{ea} (Fig. 2), that is:

$$V_{pk} = V_{ea} \tag{6}$$

As a result, the controller will adjust the V_{pk} value such that the output voltage will be maintained at the desired level for any given power level.

The proposed idea of the APFC with Amplitude Modulated Triangular Carrier is well suited for simple implementation with existing off-the-shelf ICs which permits both the regulation of the triangular carrier signal amplitude and manipulation of the PWM comparator inputs into the complementary form required to generate the Off-Duty Cycle D'.

IV. Implementation of the Triangular Carrier Generator

The proposed Amplitude Modulated Triangular Carrier Generator shown at Fig. 3 is a modification of a well known classical PWM modulator used in DC-AC inverters. Operation of this circuit is based on the principle of charging and discharging a capacitor by a positive current source and a negative current sink respectively. The programmable current source and sink are implemented by current mirrors. The current magnitude is set by the error amplifier voltage, V_{ea}, and the scaling resistor, R_T, as follows:

$$I_H = I_L = \frac{V_{ea}}{R_T} \tag{7}$$

When the S_H switch is ON and S_L is OFF, the timing capacitor, C_T, charges at a rate set up by the I_H current source. Once the capacitor voltage reaches the upper threshold, set by the error amplifier voltage, V_{ea}, the output of C_S comparator changes state and sets the S-R flip-flop (SRFF) thereby flipping S_H to OFF and S_L to ON. This will initiate the discharging of the timing capacitor, C_T, at a rate set by the current sink, I_L. Once the capacitor voltage reaches the lower threshold, which is zero, the C_R comparator resets the SRFF and the cycle is repeated. Since the charging and discharging currents are of equal magnitude, the capacitor voltage is a symmetrical triangle waveform with peak amplitude of V_{ea}. The difference between the proposed operation of the circuit and the way is normally used in a triangular PWM modulator, is in the peak

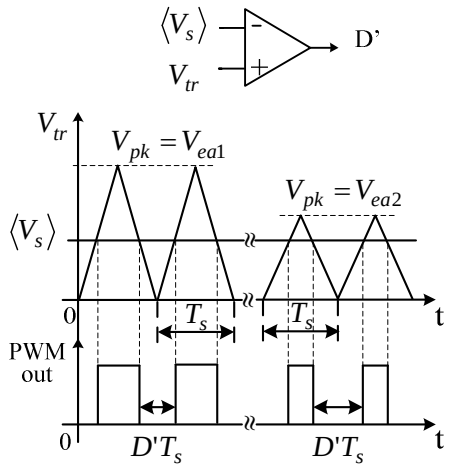

Figure 2. Proposed OFF-Duty cycle signal generation technique, for single phase Boost based APFC with no sensing of input voltage.

value of V_{ea}. In the classical circuit, this value is kept constant while in proposed circuit implementation it is variable – a function of the outer loop error signal. It should be noted however, that even though V_{ea} is not constant, the carrier period, given by:

$$T_s = 2C_T \frac{\Delta v_c}{I_{H/L}} = 2C_T \frac{V_{ea}}{\left(\frac{V_{ea}}{R_T} \right)} = 2R_T C_T \tag{8}$$

is independent of the peak voltage, V_{ea} whereas in the classical circuit implementation the frequency and the peak value of V_{ea} are correlated. Eq. (8) shows that for a slowly varying modulating signal, V_{ea}, (relative to the carrier frequency) the proposed circuit (Fig. 3) will produce an Amplitude Modulated Triangular waveform of constant frequency.

Off-the-shelf PWM modulators ICs are well suited for the implementation of the proposed idea of the APFC with Amplitude Modulated Triangular Carrier (Fig. 4). As shown below, a commercial IC (UC3637, TI) includes all the required circuitry implementing the proposed APF control,

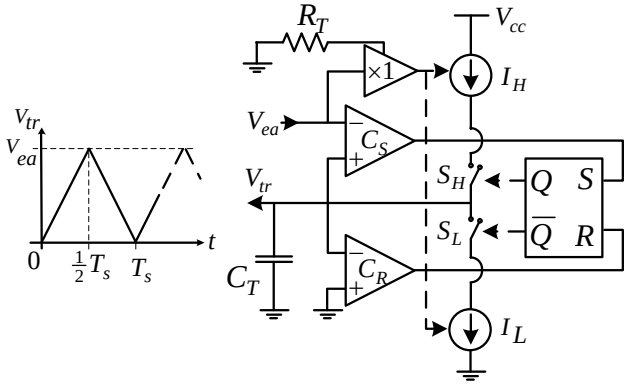

Figure 3. Schematics of the proposed Triangular Carrier Generator, for Single phase Boost based APFC with no sensing of input voltage. Current mirror currents, I_H and I_L, are scaled by R_T.

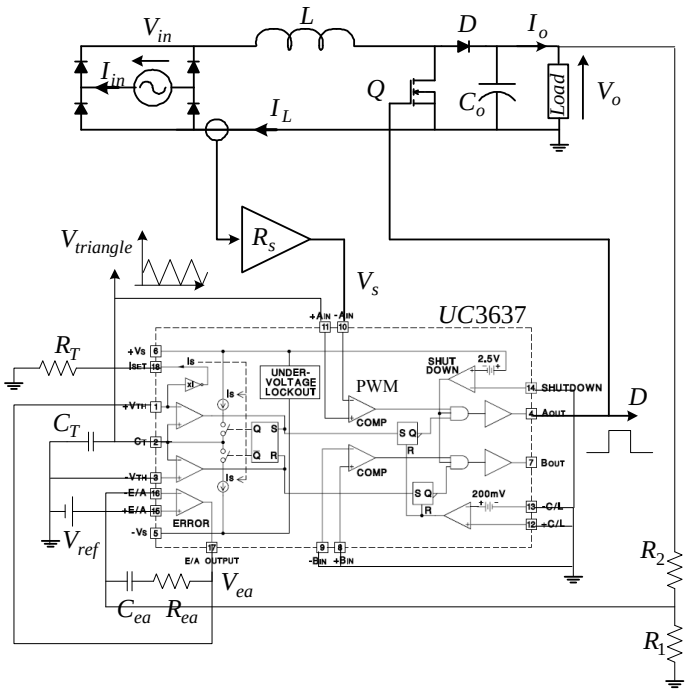

Fig. 4. Schematics of the proposed APFC.

such as control of the amplitude of the triangular carrier signal and conversion of the PWM comparator output into the complementary form (required to generate the Off-Duty Cycle D'). The simplicity of the suggested APFC is evident.

V. Comparison of APFC performance with Sawtooth and Triangular Cariers

The major difference between the modulation method proposed here and the one described in earlier studies is the shape of modulation carrier. In previous studies [10 -14] a ramp type carrier was used whereas this study proposes the application of a triangular carrier. In the ideal case, the two methods should function identically as far as the implementation of (2) is concerned. A closer examination reveals, however, that the sawtooth ramp type carrier is prone to at least two errors. One is caused by the residual ripple of the inductor current and the other from the finite time it takes the sawtooth ramp carrier to reset. As discussed below, the triangular carrier is superior to the sawtooth ramp type in these two aspects.

As illustrated in Fig. 5 (a), for the ramp carrier case, current ripple causes the Off-Duty cycle, D', to deviate by some increment, δ, from the required value. For this reason, PWM with a sawtooth carrier generates a distorted line current. The greater the ripple the greater the distortion will be. PWM comparator signals with a Triangular carrier having a leading slope, (m), and a trailing slope, $(-m)$, are shown at Fig. 5 (b). Due to the symmetry of the carrier waveform, both the leading and the trailing edges make up an angle, α, relative to the vertical axis, and an angle, β, relative to the horizontal axis as illustrated at Fig. 5 (c). The marked triangles are of equal height, Δ/2, all of their angles are equal and therefore the triangles are congruent. Accordingly, the horizontal sides are of equal length, δ. For that reason, the ripple, Δ, superimposed on the average current sense signal, $<v_s>$, advances the comparator decision point on both the leading and the trailing edges by the same instance, δ, so that an error on the leading edge is precisely compensated by the error on the trailing edge. As a result, even in the presence of a relatively large ripple, PWM comparator with Triangular carrier introduces some phase lead but otherwise generates the correct Off-Duty cycle equal to the ideal rippless case.

Aside from the ability to better cope with the residual ripple, the triangular shaped carrier improves the accuracy of the generated off duty cycle as compared to the sawtooth ramp shaped carrier in yet another way. The sawtooth ramp fall-time is finite and wastes a fraction of the switching cycle. Consequently, the generated Don, and hence the complementary, Doff, deviates from the ideal ratio of (4). This type of error does not occur in the case of modulation based on the triangular shaped carrier since no reset time is required.

When designing the current sensing network, R_S, the following issues should be considered.

Firstly, employing a low-pass type current sensing network, categorizes the system as Average Current Mode (ACM) type of control [15]. Operation in ACM is advantageous to avoid

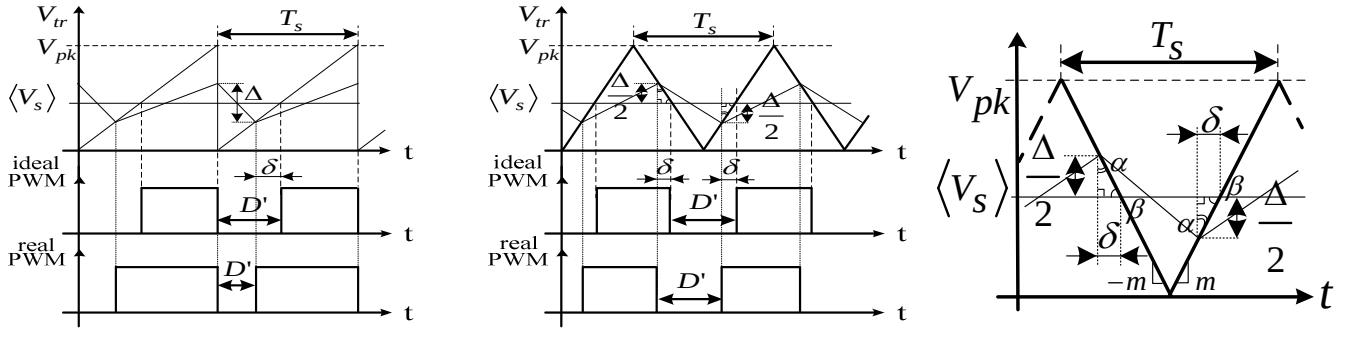

Figure 5. Comparison of PWM waveforms: Sawtooth carrier (a); Triangular carrier (b); Error compensation mechanism of triangular carrier (c).

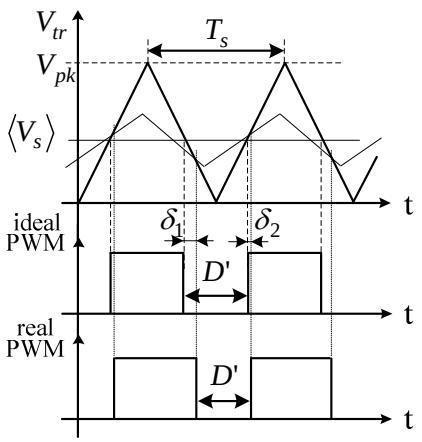

Figure 6. Off-Duty Cycle with Phase Lagging ripple.

the sub-harmonic oscillation problems and to better cope with DCM operation at low power levels. Secondly, the current sensing network should have a sufficient low-frequency gain to allow the APFC supplying full rated power, P_{Omax}, at low line condition, V_{rms_min}. Therefore, R_S should be selected according to (5) and (6) as

$$R_s = AR_{sense} = \left(\frac{V_o}{V_{rms\_min}^2} \right) \frac{V_{eamax}}{AP_{omax}} \qquad (9)$$

here, R_{sense} is the current sensing resistor, A is the current sense amplifier gain, if used, and V_{eamax}, is the saturation limit of the voltage error amplifier.

Thirdly, the current sensing network should provide sufficient current loop bandwidth. Inadequate current loop bandwidth creates distortion in the line current due to the tracking problems. Placing the pole of the current sensing network transfer function at about 1.5-2 KHz is satisfactory to ensure a negligible level of distortion [15].

Lastly, one should bear in mind that the low-pass current sensing network also introduces a 90^0 phase lag at the switching frequency. Phase shifted ripple causes Doff errors to appear as shown at Fig. 6. In order to take the full advantage of the triangular carrier ability to improve the tracking performance of the current loop, it is important to restore the phase of the current ripple. This can be achieved by introducing a high frequency zero to the current sensing network trans-impedance function to obtain a near zero phase-

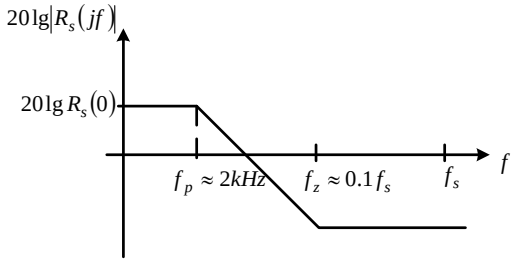

Figure 7. Suggested transfer function of the current sensing network.

shift at the switching frequency [16]. To take the full effect, the zero should be placed about a decade lower than the switching frequency. The suggested frequency response of the trans-impedance function of the current sensing network is shown in Fig. 7.

VI. Simulation Results

To simulate an exact response of the proposed APFC, a PSIM simulation of the APFC with a closed current loop was run cycle by cycle at the switching frequency. APFC design specs for simulation were: output voltage, V_O=190VDC; max output power, P_O=500W; line voltage 110Vrms/60Hz. The Boost inductor was chosen as: L=1mHy. The switching frequency was set to f_S=20kHz. Current sensing constant: R_S=1Ω. Ramp and control voltages at full power were: V_{pkmax}=V_{eamax}=7v. In this simulation, the inductor current was applied as-is to the PWM comparator, without filtering (peak-current mode).

The simulated waveforms of the normalized line voltage and current are shown in Fig. 8 and stand in a good agreement with theoretical expectations. The simulated APFC operated in CCM throughout the line half-cycle. The input current of the APFC with Sawtooth ramp, shown in Fig. 8 (a), is distorted due to the Off-Duty Cycle error induced by the current ripple, whereas the current of the APFC with Triangular carrier tightly follows the line voltage as shown in Fig. 8 (b).

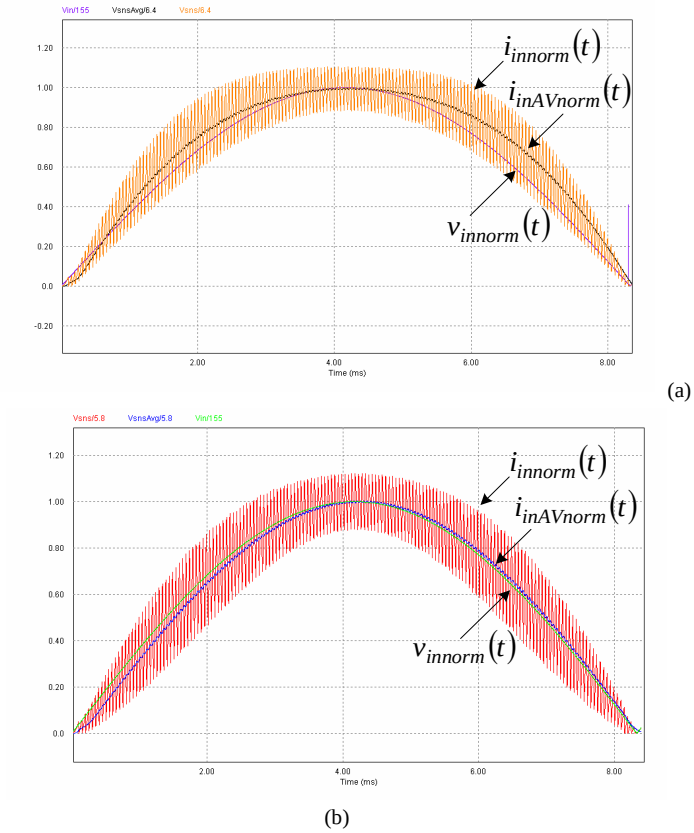

Figure 8. Comparison of APFC tracking performance: simulated waveforms of the Normalized Line voltage, $V_{innorm}(t)$, the Normalized instantaneous Line current, $i_{innorm}(t)$, and the Normalized filtered/averaged Line current, $i_{inAVnorm}(t)$: APFC with Sawtooth ramp (a); APFC with Triangular carrier (b).

VII. EXPERIMENTAL RESULTS

The two modulation methods, with a sawtooth ramp and triangular shaped carriers were tested experimentally using the same Boost power stage. The power stage was based on an evaluation board [17] designed to achieve: 380VDC/300W at 220Vrms line. The Boost stage was operated at f_s=100kHz switching frequency, inductor and capacitor used were L=1mHy and C=330µF. The sawtooth ramp type control was implemented with an ASIC controller [18] while the triangular carrier modulator was built around an off the shelf IC UC3637 (TI), as shown in Fig. 4. Measured waveforms are shown in Fig. 9, 10 and 11. Performance indexes are summarized in Table 1. In all cases the control performed as predicted, especially at the nominal power level Fig. 11. The relatively higher distortion at the low power level is due to the DCM nature of the inductor current. It should be recalled that the control law (2) is theoretically correct only for the CCM case. Experimental results stand in good agreement with presented theory.

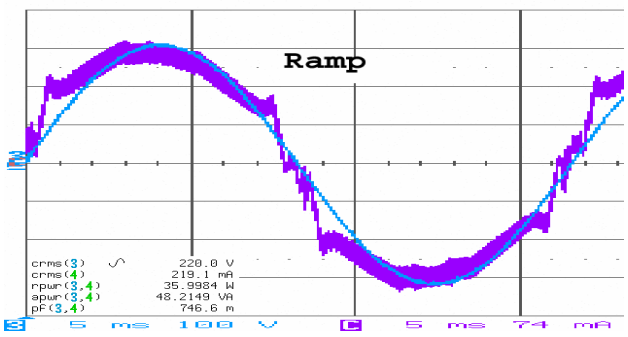

(a)

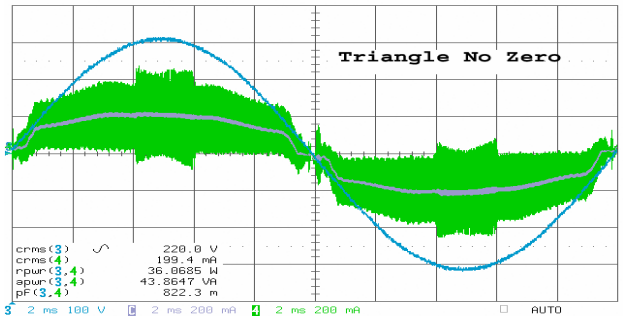

(b)

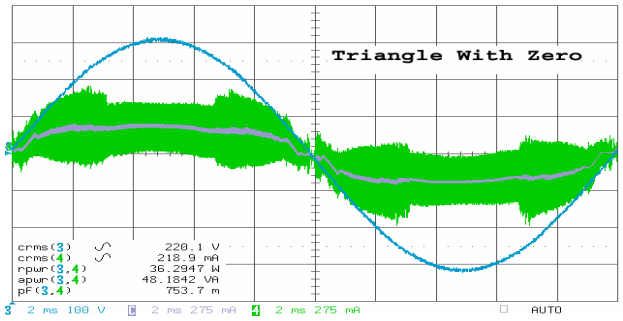

(c)

Figure 9. Comparison of Experimental APFC waveforms at power level of 36 Watts: sawtooth ramp-(a), Vertical scales: 100V/Div; 0.74Amp/Div; Triangular carrier with current compensator that includes NO zero-(b), Vertical scales: 100V/Div; 0.2Amp/Div; Triangular carrier with current compensator that includes a ZERO-(c). Blue – Input Voltage; Green – Unfiltered input current; Violet – average input current. Vertical scales: 100V/Div; 0.275Amp/Div.

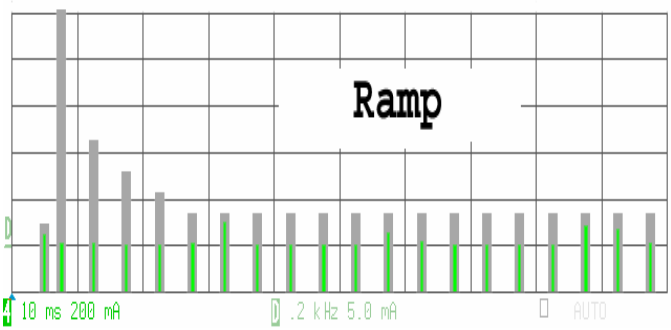

(a)

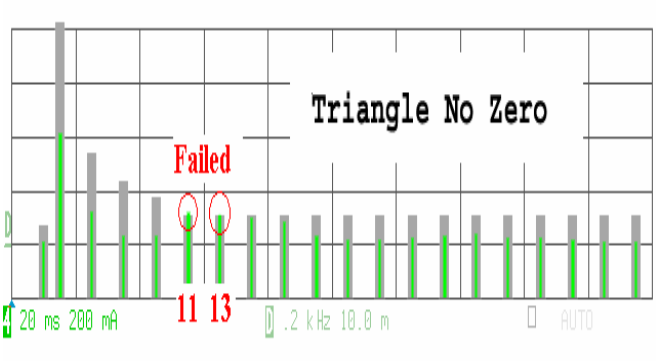

(b)

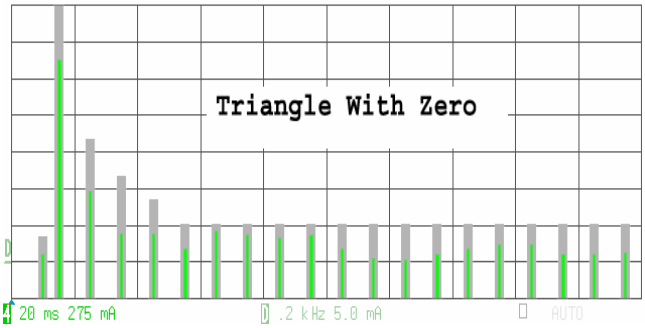

(c)

Figure 10. Experimental APFC waveforms: Harmonic Standard Compliance at power level of 36 Watts: sawtooth ramp-(a); Triangular carrier with current compensator that includes NO zero-(b); Triangular carrier with current compensator that includes a ZERO-(c). Grey – Class-C standard limit; Green – Measured input current amplitude (Harmonics: 2, 3, 5, 7…)..

TABLE I
SUMMARY OF MEASURED PF AND CLASS-C STANDARD COMPLIANCE

APFC TYPE \ POWER LEVEL	12.5W	36W	160W	294W
Triangle Carrier (No-Zero)	0.632 Pass	0.822 *Fail*	0.8969 Pass	0.9649 Pass
Triangle Carrier (Added Zero)	0.6688 Pass	0.7537 Pass	0.9183 Pass	0.9718 Pass
Ramp	0.2747 *Fail*	0.7466 Pass	0.982 Pass	0.9931 Pass

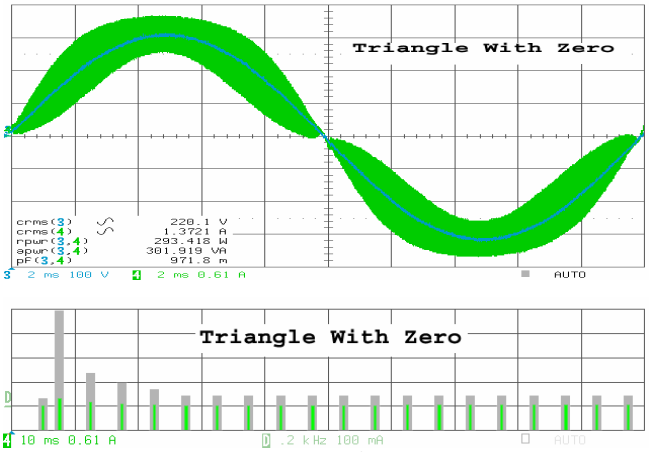

Figure 11. Experimental APFC unfiltered input current, voltage waveforms and Harmonic Standard Compliance at power level of 294 Watts; Triangular carrier with current compensator that includes a ZERO. Upper graph: Blue – Input Voltage; Green – Unfiltered input current. Vertical scales: 100V/Div; 0.61Amp/Div. Lower graph: Grey – Class-C standard limit; Green – Measured input current amplitude (Harmonics: 2, 3, 5, 7…)..

VIII. CONCLUSIONS

This paper presented an alternative Active Power Corrector control scheme without line voltage sensing based on a CCM Boost converter. The proposed APFC employs amplitude modulated triangular carrier to control the average input current and power level. The control circuits of the experimental APFC are simple and were implemented with existing off-the-shelf ICs. The theoretical predictions are well supported by simulation and experimental results. The experimental APFC proved to be stable and robust. The APFC tracking performance with triangular carrier was found to be similar to that of the saw tooth ramp carrier. Some differences can be seen at the low power level were the proposed APFC control exhibits a lower line current distortion. This difference is insignificant however from the practical point of view since low power systems are exempt from the line harmonics standards. The reason for the small, if at all, improvement is probably due to current filtering used in the experiments. Evidently, with a reduced inductor current ripple, the performance of the triangular and sawtooth ramp carrier modulators is about the same. The proposed triangle based APFC control scheme can thus be considered as an alternative approach to previously suggested methods.

REFERENCES

[1] R. Redl, P. Tenti and J.D. Van WYK, *"Power Electronics' Polluting Effects,"* IEEE Spectrum, May 1997, pp.32-39

[2] *"IEEE 5I9 Recommended Practices and Requirements for Harmonic Control in Electrical Power Systems,"* IEEE Industry Applications Society/ Power Engineering Society, 1993.

[3] Limits for Harmonic Current Emissions (Equipment Input Current<16A per Phase), IEC 1000/3/2 Int. Std., 1995.

[4] J. Sebastian, M. Jaureguizar and J. Uceda, "An overview of power factor correction in single-phase off-line power supply systems", IECON '94, vol.3, pp. 1688 – 1693.

[5] C. Qiao, K. M. Smedley, *"A Topology Survey of Single-Stage Power Factor Corrector with a Boost Type Input-Current-Shaper," IEEE Trans. on Pow. Electron*, vol. 16, Issue 3, May 2001, pp. 360-368.

[6] J. C. Salmon, *"Techniques for Minimizing the Input Current Distortion of Current-Controlled Single-phase Boost Rectifiers," IEEE Trans. on Pow. Electron*, vol. 8, no. 4, October 1993, pp. 509-520.

[7] O. Garcia, J. A. Cobos, R. Prieto, P. Alou, J. Uceda, *"Single Phase Power Factor Correction: A Survey", IEEE Trans. on Pow. Electron.*, vol. 18, Issue 3, May 2003, pp. 749-755.

[8] D. Maksimovic, Y. Jang and R. W. Erickson, "Nonlinear carrier control for high power factor boost rectifiers", *IEEE Trans. on Pow. Electron.*, vol. 11, no. 2, pp. 578-584, July 1996.

[9] J. Gegner and C. Q. Lee, "Linear peak current mode control: a simple active power factor correction control technique for continuous conduction mode", in *Conf. Rec. IEEE PESC'96*, 1996, pp. 196-202.

[10] Z. Lai and K. Smedley, "A family of power factor correction controllers", *IEEE Trans. on Pow. Electron.*, vol. 13, Issue: 3, May 1998, pp.: 501 - 510.

[11] Y. Liu and K. Smedley, "Control of a dual boost power factor corrector for high power applications", IECON '03. Pages: 2929 – 2932.

[12] J. Rajagopalan and F. C. Lee, "A generalized technique for derivation of linear average current mode control laws for power factor correction without input voltage sensing", in *Conf. Rec. IEEE APEC'97*, 1997, pp. 81-87.

[13] S. Ben-Yaakov and I. Zeltser, "PWM Converters with Resistive Input", *IEEE Trans. Ind. Electron.*, vol. 45, no. 3, pp. 519-520, June1998.

[14] S. Ben-Yaakov and I. Zeltser, "The Dynamics of a PWM Boost Converter with Resistive Input", *IEEE Trans. Ind. Electron.*, vol. 46, no. 3, pp. 613-619, June1999.

[15] L. Dixon, "Average Current Mode Control of Switching Power Supplies", Unitrode application note U-140.

[16] A. Abramovitz and S. Ben-Yaakov, " Current spectra translation in single phase rectifiers: implementation to active power factor correction", *IEEE Trans. Circuits and Systems: I. Fundamental Theory and Applications*, 44, No. 8, 771-775, 1997.

[17] Green Power Technologies Ltd, GPTC1104X evaluation board, http://www.g-p-t.com/Papers/EVBGPTC1104X-DES_2005.pdf

[18] Green Power Technologies Ltd, GPTC110XX data sheet, http://www.g-p-t.com/Papers/GPTC1105X_2005.pdf